Optimizing Oxygen Vacancy Concentration and Electronic Transport Processes in the Mn_xCo/CeO_2 Nanoreactor: Regulation Mechanism of Radical to Non-radical Pathway

Hailan Qin[a], Jiahao Wang[a], Siyuan Di[a], Yunkang Liu[a], Pin Chen[a], Min Liu[a], Qiuyue Zhang[a], and Shukui Zhu[*a]

[a] State Key Laboratory of Biogeology and Environmental Geology, China University of Geosciences, Wuhan 430074, China.

[*] Corresponding author. E-mail: shukuizhu@126.com; phone: +86-27-67883452

ORCID：Shukui Zhu: 0000-0002-4563-6681

Synthesis of CeO_2

CeO_2 was prepared using the facile hydrothermal calcination method. Initially, 6 mmol of $Ce(NO_3)_3·6H_2O$ was dissolved in 100 mL of deionized water by ultrasound at room temperature. The solution was then transferred to a thermostat water bath. Next, 4 mL of $NH_3·H_2O$ was added to the aforementioned solution. The mixture was stirred for 2 h at 40 °C and aged for 12 h. The resulting precipitate was washed several times with ultrapure water and ethanol absolute, and then dried in a vacuum freeze drier. Finally, the treated powder products were heated at 300 °C for 2 h at a heating rate of 2 °C/min in a tubular furnace.

Synthesis of Co/CeO_2 or Mn/CeO_2

Co/CeO_2 or Mn/CeO_2 catalyst was synthesized by hydrothermal calcination method. Firstly, 6 mmol of $Ce(NO_3)_3·6H_2O$ and 2 mmol of $CoCl_2·6H_2O$ or $MnCl_2·4H_2O$ were comprehensively dissolved in 100 mL of deionized water. Secondly, 4 mL of $NH_3·H_2O$ was rapidly added to the above solution. Thirdly, the aforementioned suspensions were transferred to a water bath (40 °C) and stirred for 2 h, followed by aging for 12 h. Subsequently, the resulting product was washed with ultrapure water and ethanol absolute, before being dried using a vacuum freeze dryer. Finally, the prepared products were heated in a tube

furnace (300 ° C, 2 ° C/min, 2 h).

Catalyst Characterization

The XRD patterns of the synthesized samples were analyzed using a Bruker X-ray Diffractometer (Germany). The specific surface area and pore size were obtained by BET on a Micromeritics ASAP 2460 (USA) instrument. The morphology and microstructure of the samples were examined using a Hitachi S4800 FEG SEM and Tecnai G2 20 TEM. X-ray photoelectron spectroscopy (XPS) analysis was performed using a Thermo Fisher Scientific ESCALAB 250XI spectrometer to characterize the chemical composition and chemical environment of as-samples. Elemental analysis and metal leaching were conducted using an Agilent 730 inductively coupled plasma optical emission spectrometer (ICP-OES), with the sample being dissolved in a strong acid solution prior to testing. The contact angle meter was obtained by an Angle Contact Metering System (XG-CAM). Electron spin resonance spectroscopy (ESR) was conducted using a Bruker EMXPLUS spectrometer. The AutoChem II 2920 apparatus was used to perform oxygen temperature-programmed desorption (O_2-TPD) and hydrogen temperature-programmed reduction (H_2-TPR).

Catalytic Activity Evaluation

CIP was selected to evaluate the catalytic performance of Mn_xCo/CeO_2. Specifically, a mixture containing 300 mg/L of catalytic sample, 100 mg/L of PMS, and 50 mL of CIP (10 mg/L) aqueous solution was stirred uniformly for 50 min at room temperature in a quartz tube. Subsequently, the mixed solution was taken at regular intervals and passed through a 0.22 μm pinhole filtration membrane for filtration. The concentration of CIP was monitored using a METASH UV-5100B spectrophotometer at 276 nm. To calculate the actual degradation efficiency, formula S1 was employed after converting the

absorbance and concentration values. Furthermore, all degradation experiments were conducted using ultrapure water as the solvent.

Calculation method of CIP removal rate: the corresponding removal rate of CIP was calculated by the following formula S1.

$$\eta\ (\%) = (C_t/C_0) \times 100$$

Where C_0 is the initial concentration of CIP in solution, C_t is the CIP concentration under different reaction time, η is the pollutant removal rate.

Texts

Text S1. Materials

All reagents were analytical grade and without further purification. Cerium nitrate hexahydrate ($Ce(NO_3)_3 \cdot 6H_2O$) furfuryl alcohol (FFA), and ciprofloxacin (CIP) were furnished by Macklin Biochemical Co., Ltd. Cobaltous chloride ($CoCl_2 \cdot 6H_2O$), tert-butanol (TBA), and tetracycline(TC) were obtained from Aladdin Biochemical Technology Co., Ltd. Manganese chloride tetrahydrate ($MnCl_2 \cdot 4H_2O$), ammonium hydroxide (NH_4OH), ethanol, ethylenediamine tetra acetic acid disodium salt (EDTA-2Na), p-benzoquinone (PBQ), methanol, and rhodamine B (RhB) were purchased from Sinopharm Chemical Reagent Co., Ltd. Chlortetracycline (CTC) and oxytetracycline (OTC) were provided by Meryer (Shanghai) Chemical Technology Co., Ltd.

Text S2. DFT calculations

First-principles calculations in the framework DFT are performed by using the Vienna Ab Initio Simulation Package (VASP) with the projector-augmented wave method (PAW).[1] The exchange-correlation energy was calculated by using the generalized gradient approximation (GGA) of Perdew-Burke-Ernzerhof (PBE).[2] To correct the van der Waals interactions, the DFT-D3 method proposed by Grimme *et al.* was adopted.[3] The energy cutoff is set to 400 eV. Spin polarization effects are considered in this study. We performed structural optimization until the residual forces on each ion converged to less than 0.01 eV

Å^{-1}. A 3 × 3 surface unit cell was used for the CeO_2 (111) surface. The Mn_xCo/CeO_2 was constructed by replacing one of the surface Ce atoms with a Co or/and Mn atom. Oxygen vacancy was modeled by removing one oxygen atom from a unit cell. The adsorption energy for surface PMS adsorbates is defined as follows: $\Delta E_{PMS} = E_{adsorption} - E_{surface} - 0.5 \times E_{PMS}(g)$, where $E_{adsorption}$ represents the energy of the surface with the adsorbed PMS, $E_{surface}$ represents the energy of the pure surface, and $E_{PMS}(g)$ represents the energy of the PMS species in the gas phase. The calculation also includes entropy (S) and zero-point energy (E_{ZPE}) to obtain the Gibbs free adsorption energy of PMS: $\Delta G_{PMS} = \Delta E_{PMS} + \Delta E_{ZPE} - T\Delta S$.

Text S3. Toxicity calculation

The toxicity of CIP and its oxidation process products were evaluated by the ecological structure-activity relationship (ECOSAR) predictive model. The median lethal concentration (LC50) of fish exposed to CIP for 96 h, daphnid exposed for 48 h, and median effect concentration (EC50) of green algae exposed for 96 h were calculated by this software. In the meantime, the geometric mean of the unobserved effect concentration and the lowest observed effect concentration (ChV) for fish, daphnid, and green algae were assessed. Acute toxicity was evaluated as LC50 or EC50, and chronic toxicity as ChV.

Text S4. Partial reaction

$$\cdot SO_4^- + H_2O \rightarrow \cdot OH + SO_4^{2-} + H^+ \quad \text{(S1)}$$

$$\cdot SO_4^- + OH^- \rightarrow \cdot OH + SO_4^{2-} \quad \text{(S2)}$$

$$HSO_5^- \rightarrow SO_5^{2-} + H^+ \quad \text{(S3)}$$

$$SO_5^{2-} + H_2O \rightarrow \cdot O_2^- + SO_4^{2-} + H^+ \quad \text{(S4)}$$

$$\cdot SO_4^- + OH^- \rightarrow \cdot OH + SO_4^{2-} \quad \text{(S5)}$$

$$\cdot OH + OH^- \rightarrow \cdot O_2^- + H_2O \quad \text{(S6)}$$

$$2\cdot O_2^- + H_2O \rightarrow 2^1O_2 + H_2O_2 + 2OH^- \quad \text{(S7)}$$

$$\cdot SO_5^- + \cdot SO_5^- \rightarrow 2SO_4^- + {}^1O_2 \quad \text{(S8)}$$

$$HSO_5^- + SO_5^{2-} \rightarrow HSO_4^- + SO_4^{2-} + {}^1O_2 \quad \text{(S9)}$$

Figures

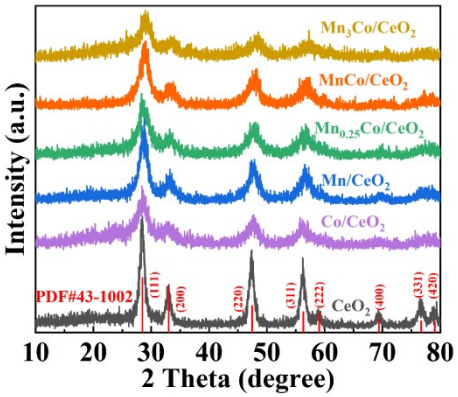

Fig. S1 XRD patterns of the synthesized catalysts.

The peaks of 2θ = 28.55°, 33.08°, 47.48°, 56.34°, 59.09°, 69.42°, 76.70°, and 79.08° were attributed to (111), (200), (220), (311), (222), (400), (331) and (420) crystal plane of CeO_2, respectively.

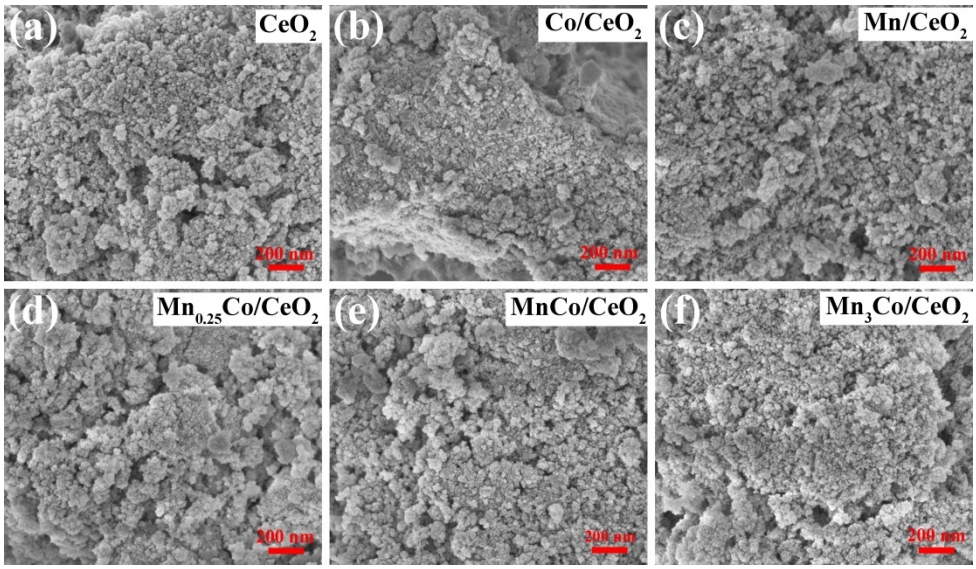

Fig. S2 SEM images of the completed samples: (a) CeO_2, (b) Co/CeO_2, (c)

Mn/CeO_2, (d) $Mn_{0.25}Co/CeO_2$, (e) MnCo/CeO_2, (f) Mn_3Co/CeO_2.

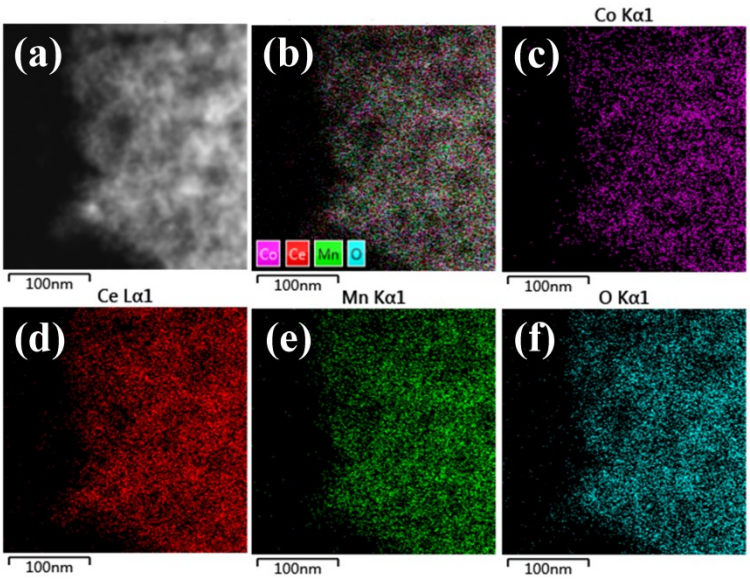

Fig. S3 (a) HAADF-STEM image and EDX mapping results of the as-prepared MnCo/CeO_2 sample, (b) all elements, (c) Co, (d) Ce, (e) Mn, (f) O.

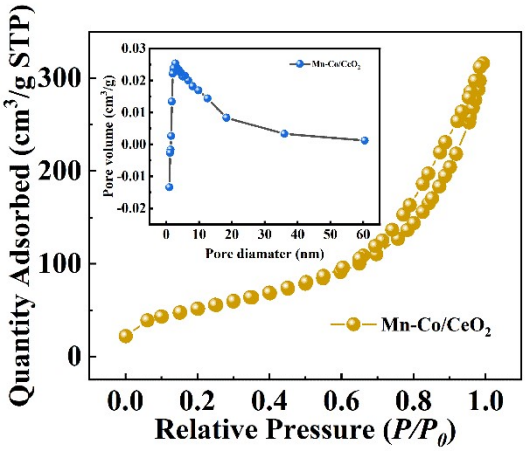

Fig. S4 Isothermal adsorption-desorption curves and the corresponding pore-size distributions (inset) of MnCo/CeO_2.

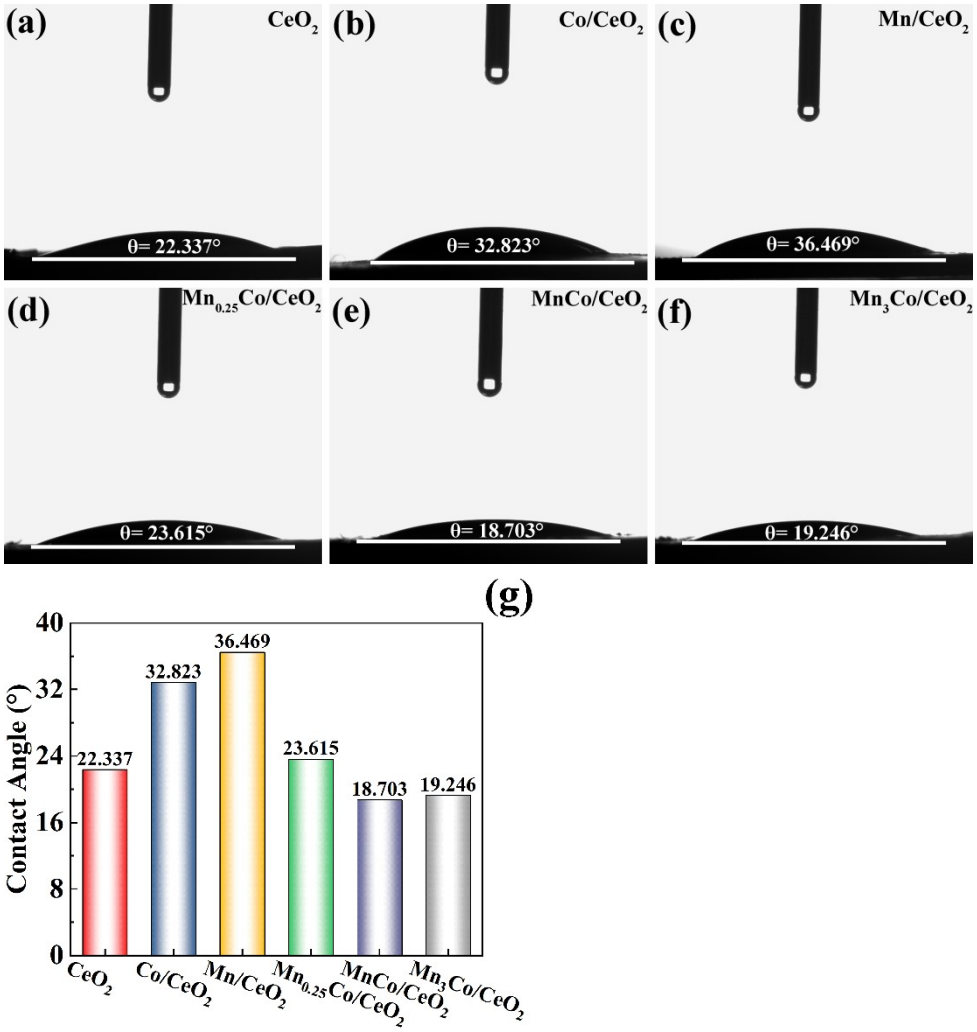

Fig. S5 Surface water contact angle measurements of as-prepared samples.

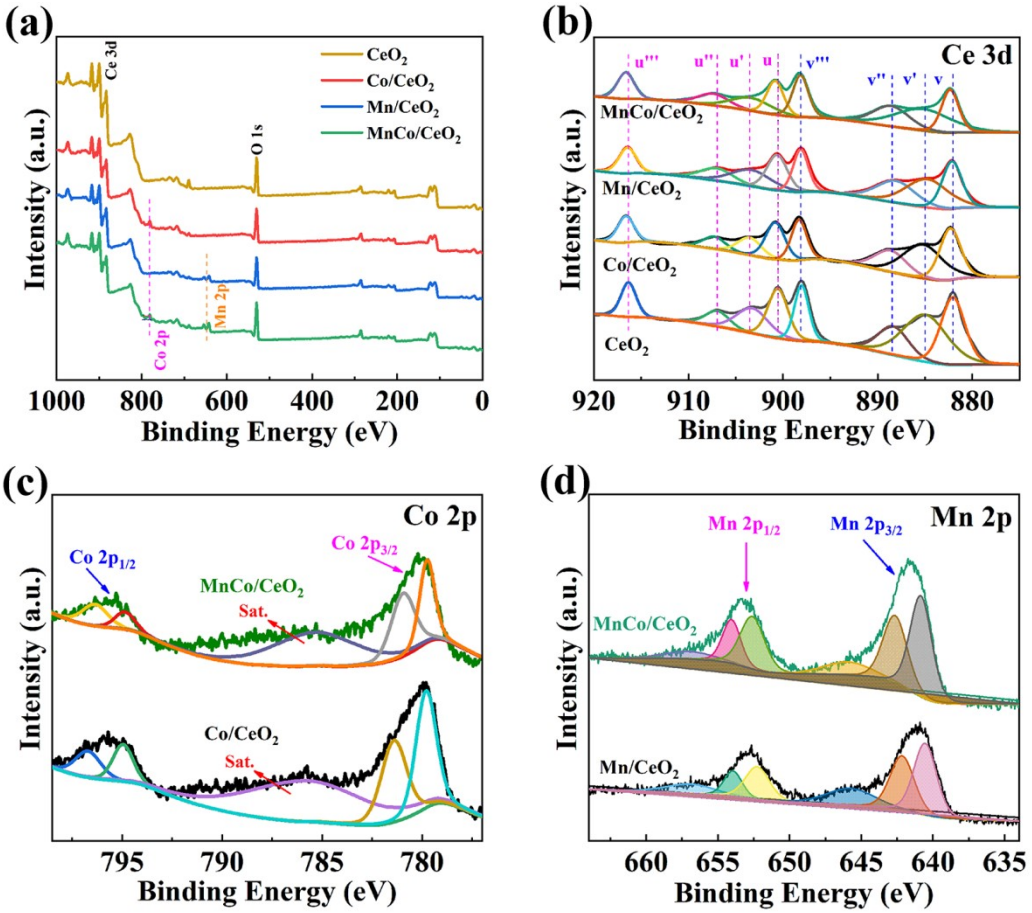

Fig. S6 XPS spectra of as-prepared samples: (a) survey, (b) Ce 3d, (c) Co 2p, (d) Mn 2p.

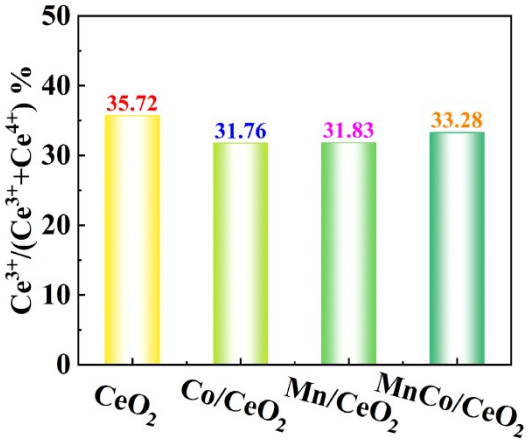

Fig. S7 The content proportion of Ce^{3+} in the synthesized sample.

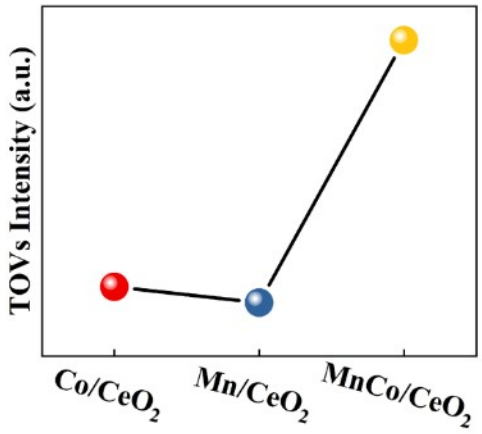

Fig. S8 Changes in TOVs concentration of the synthesized sample.

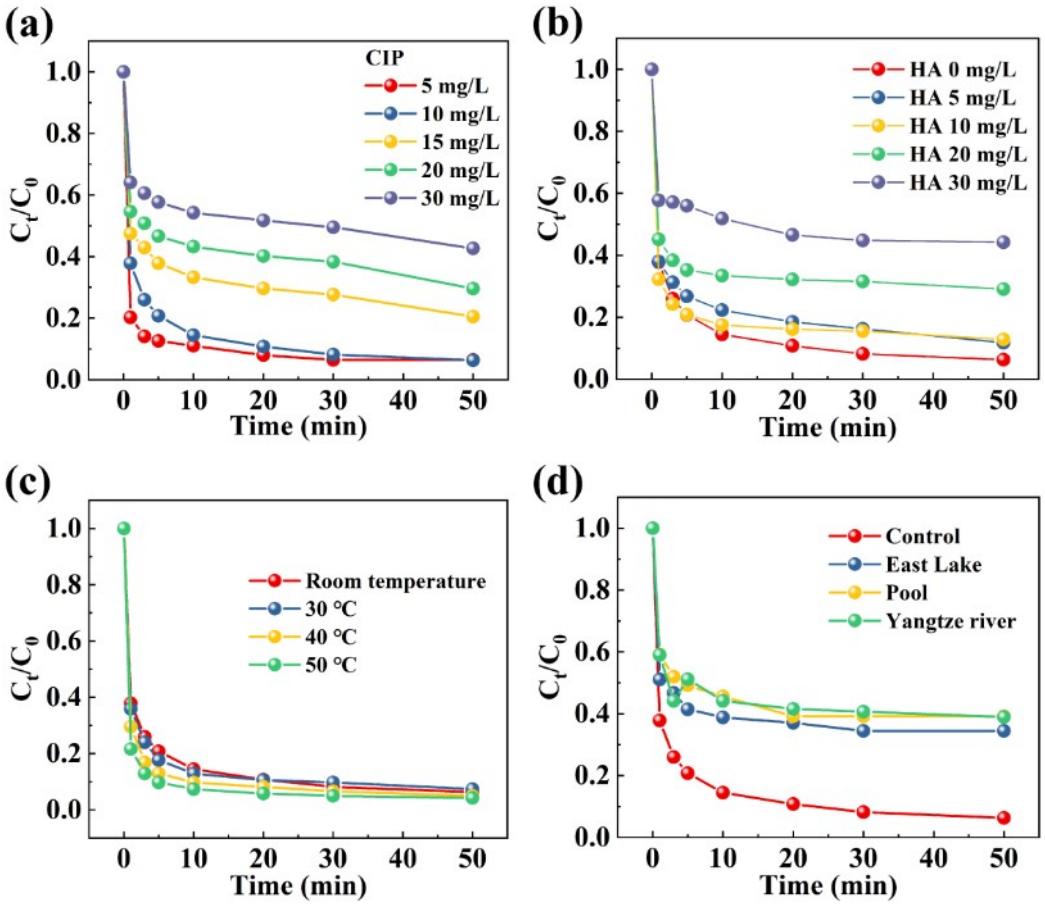

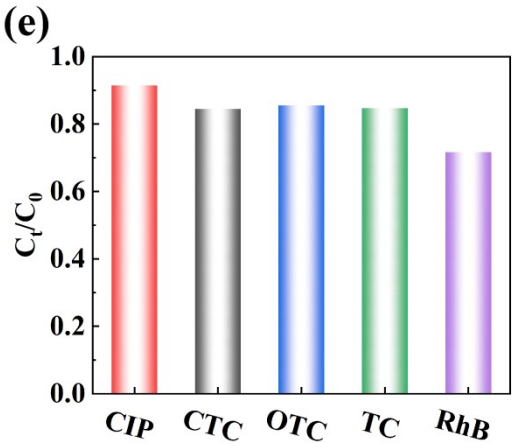

Fig. S9 Effects of different factors on CIP degradation: (a) CIP concentration, (b) HA, (c) temperature, (d) natural substrates, (e) different pollutants.

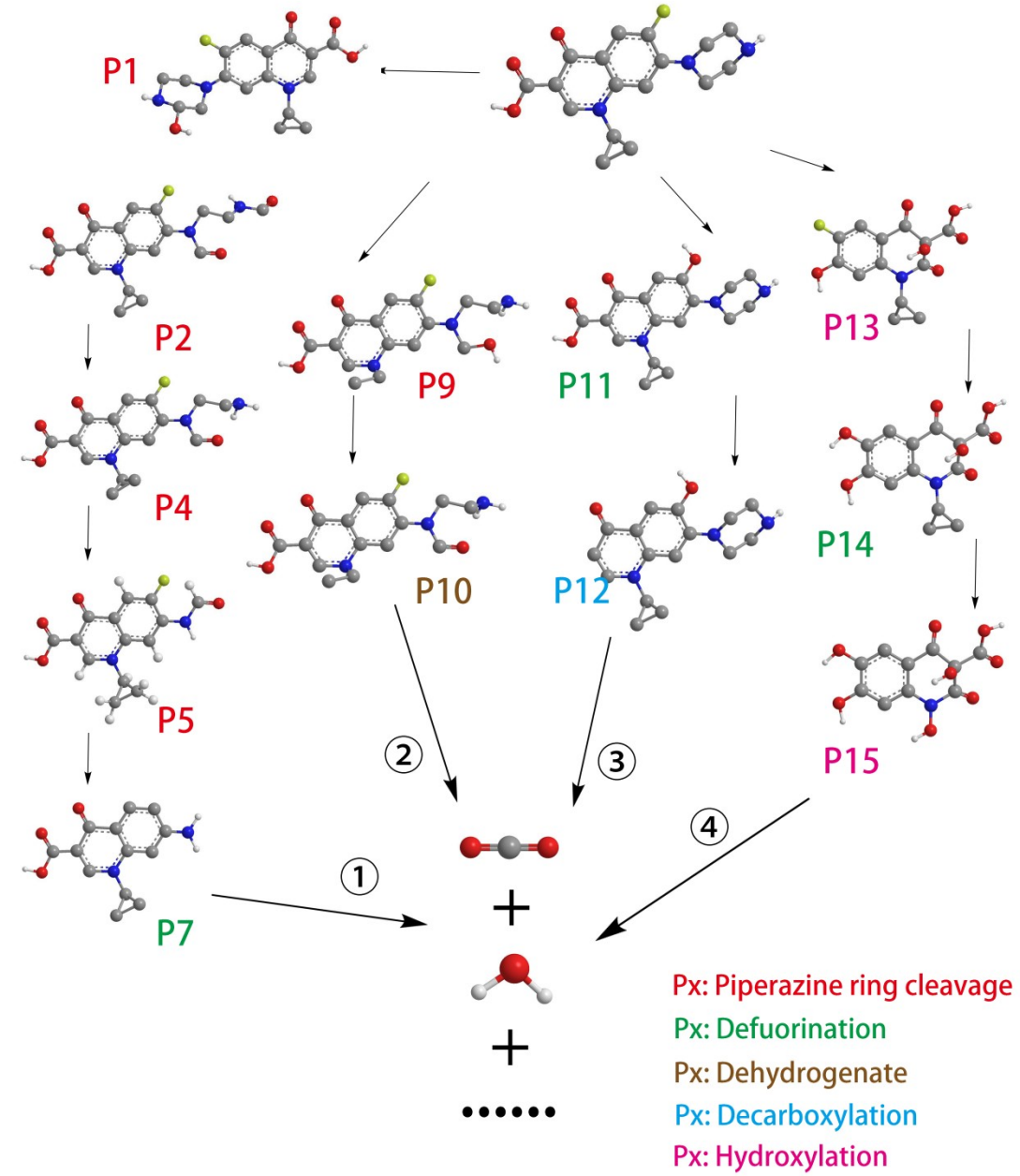

Fig. S10 Proposed degradation pathway of CIP. The O, C, F, H, and N atoms are shown in red, gray, yellow, white, and blue, respectively.

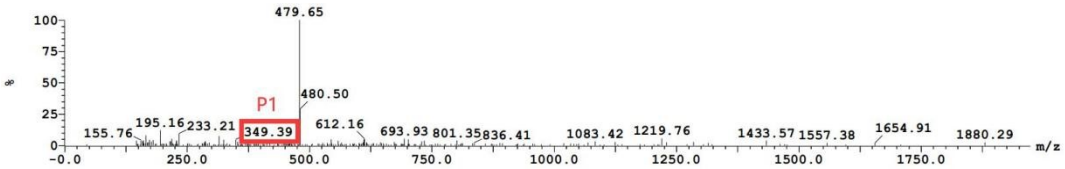

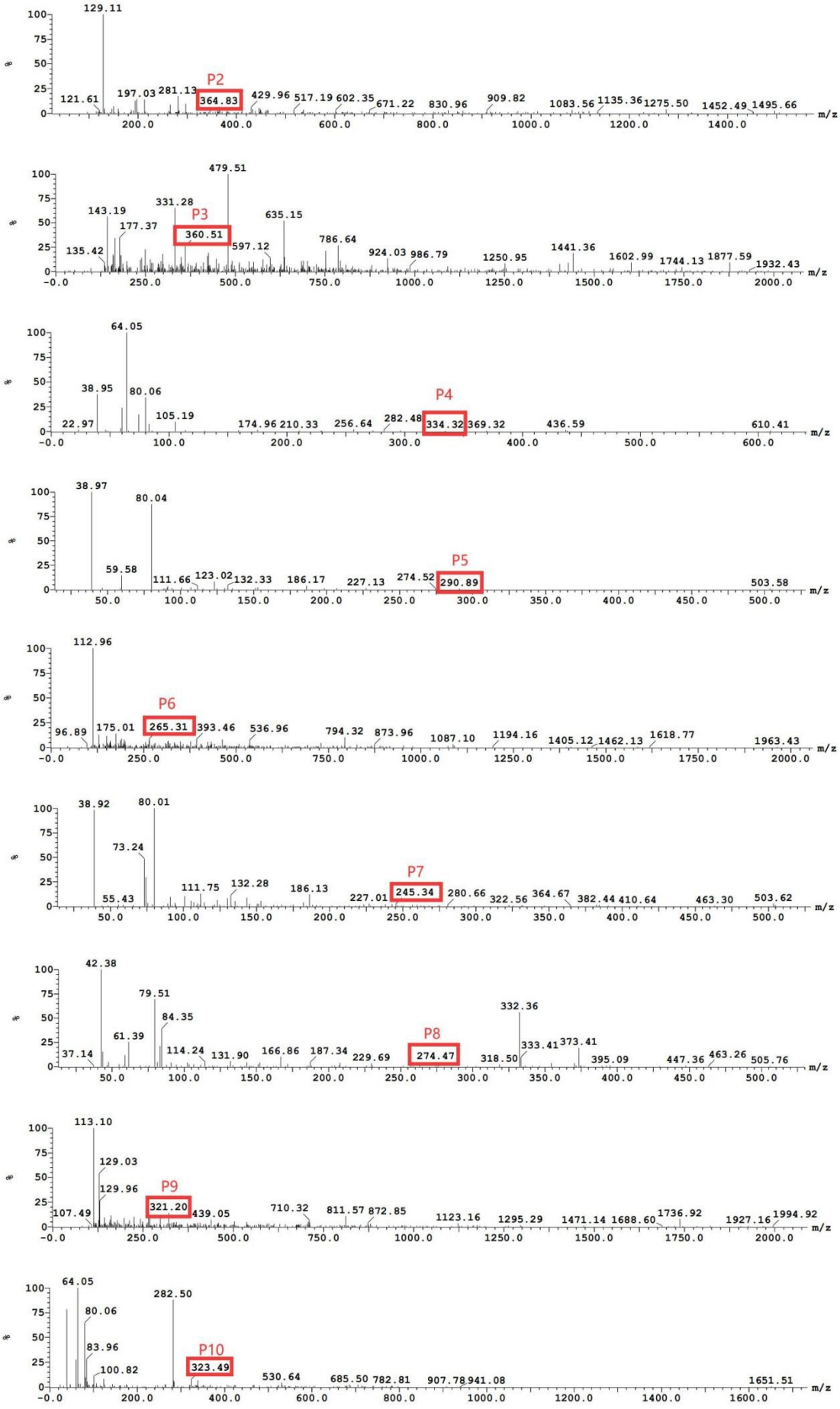
P2
364.83
P3
360.51
P4
334.32
P5
290.89
P6
265.31
P7
245.34
P8
274.47
P9
321.20
P10
323.49
m/z

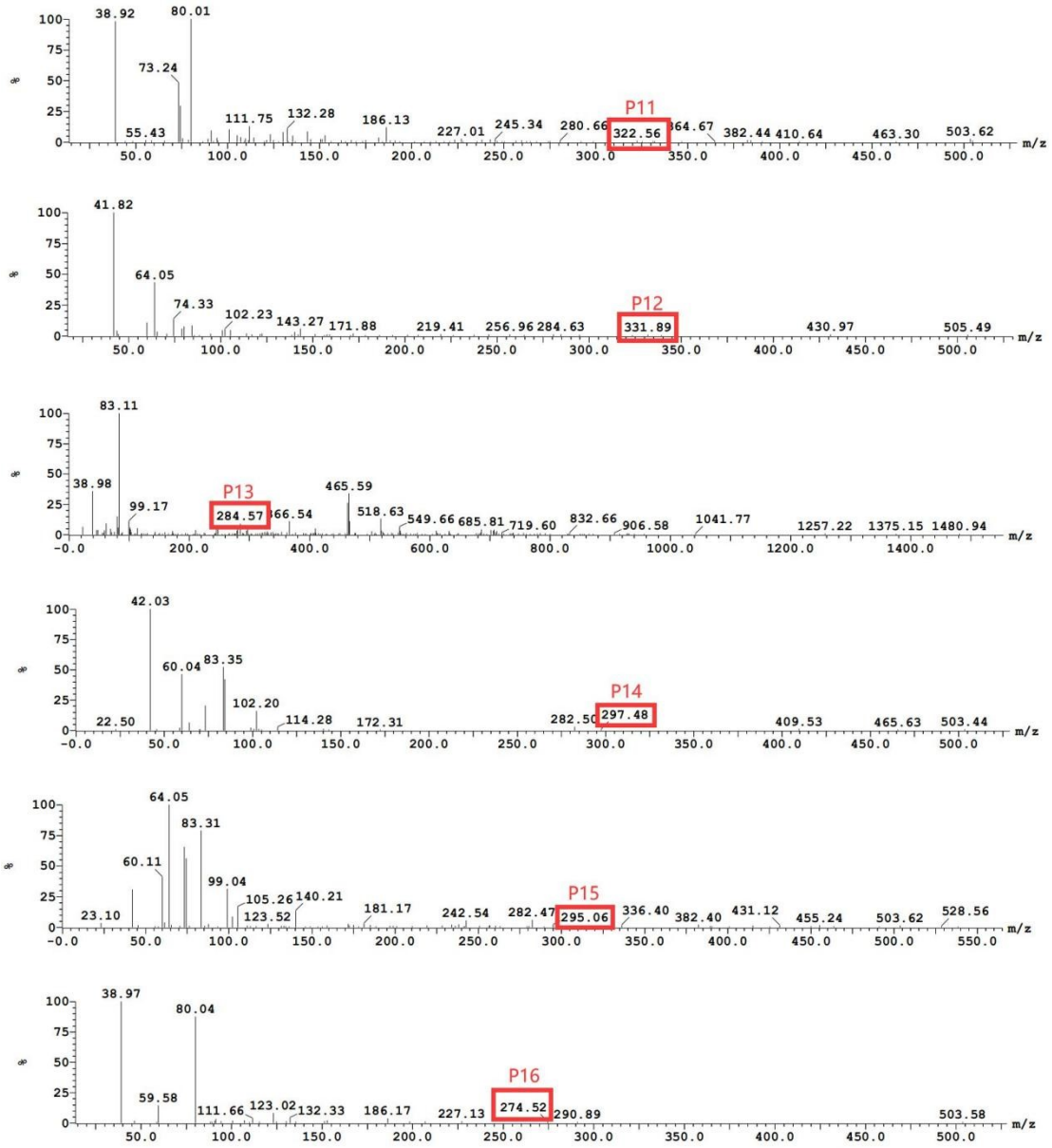

Fig. S11 Possible degradation paths of CIP oxidized by MnCo/CeO_2.

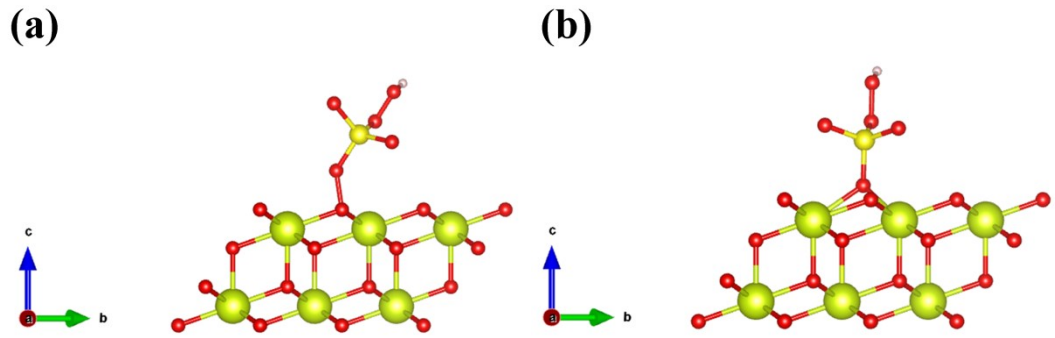

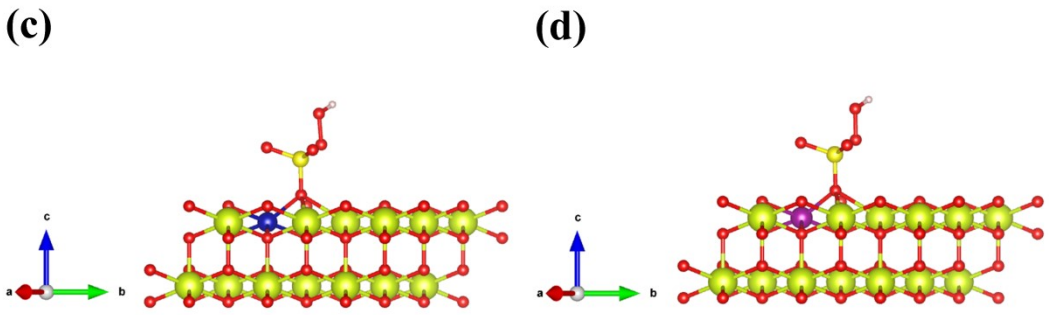

Fig. S12 Optimized configurations of PMS adsorbed on (a) traditional CeO_2 (111) substrate, (b) CeO_2 (111) substrate with OVs, (c) Co/CeO_2 (111) substratewith OVs, (d) Mn/CeO_2 (111) substrate with OVs. The O, Ce, S, H, Co, and Mn atoms are shown in red, green, yellow, pink, blue, and purple, respectively.

Tables

Table S1. Metal doping content and leaching of MnCo/CeO_2.

	Co	Mn
Metal doping content (%)	6.21%	7.51%
Metal leaching (mg/L)	0.55	0.26

Table S2. Comparison of $MnCo/CeO_2$ and reported catalysts in the catalytic performances for CIP degradation.

Catalyst	CIPconcentration	Catalysts dosage	PMS concentration	Time	Removal efficiency	Ref.
$Co_{0.6}$/N@ZS-SA	20 mg/L	6 g/L	0.5 g/L	60 min	82.5%	[4]
$CuS/Fe_2O_3/Mn_2O_3$	10 mg/L	0.2 g/L	0.6 g/L	120 min	88.0%	[5]
CoO-N/BC	10 mg/L	0.1 g/L	1 mM	60 min	84.3%	[6]
$BiVO_4$/visible light	10 mg/L	0.32 g/L	0.96 g/L	120 min	92.3%	[7]
Magnetized nitrogen-doped biochar	10 mg/L	0.8 g/L	0.2 g/L	80 min	92.6%	[8]
Co_3O_4/CeO_2/visible light	5 mg/L	0.5 g/L	0.1 g/L	50 min	87.8%	[9]
CuCo/C	10 mg/L	0.25 g/L	0.25 g/L	30 min	90.0%	[10]
$CuFe_2O_4/CuO$	5 mg/L	0.5 g/L	0.3 g/L	120 min	86.67%	[11]
$CoFe_2O$	20 mg/L	0.3 g/L	2 mM	90 min	90.0%	[12]
$MnCo/CeO_2$	10 mg/L	0.3 g/L	0.1 g/L	50 min	93.71%	This work

Table S3. Toxicity evaluation of the intermediates.

Degradation products	Acute toxicity (mg/L)			Chronic toxicity (mg/L)			Hazard category
	Fish	Daphnid	Green Algae	Fish	Daphnid	Green Algae	

			96-hr LC_{50}	48-hr LC_{50}	96-hr EC_{50}	ChV			
	CIP		0.180	0.520	1621.628	1340.500	81.270	455.221	Very toxic
	P1	m/z = 349.39	1.41e+005	11143.716	20753.244	28788.693	613.564	5121.095	Not harmful
	P2	m/z = 364.83	8.18e+005	56634.961	1.37e+005	2.49e+005	2743.711	30710.936	Not harmful
	P3	m/z = 360.51	40068.211	18276.063	1011.08	22.443	968.874	349.154	Not harmful
	P4	m/z = 334.32	1.41e+005	11096.859	5145.498	72.675	609.157	1074.013	Not harmful
I	P5	m/z = 290.89	1041.004	553.443	75.605	3.146	44.940	52.575	Harmful
	P6	m/z = 265.31	1283.546	10.067	45.480	7.059	0.535	76.908	Not harmful
	P7	m/z = 245.34	1489.554	17.838	47.278	9.150	0.571	78.405	Harmful
	P8	m/z = 274.47	366.021	203.374	138.510	34.874	18.673	34.564	Not harmful
	P9	m/z = 321.20	20081.355*	1830.796	2567.494*	2647.198*	115.882	702.540*	Not harmful
II	P10	m/z = 323.49	3.18e+005	23487.105	50043.414	79916.461	1210.392	9019.49	Not harmful
	P11	m/z = 322.56	2.16e+005	16381.941	7676.092	96.581	868.778	1408.671	Not harmful
III	P12	m/z = 331.89	1649.225	55.694	881.464	211.121!	77.646	85.932	Harmful
	P13	m/z =	14.226	1.610	5.450	0.766!	0.472	1.059	Toxic

		284.57								
	P14	m/z = 297.48	1258.178	46.236	656.997	21.300	57.804	67.214		Harmful
IV	P15	m/z = 295.06	2410.899	62.780	739.001	43.292	122.372	61.694		Harmful
	P16	m/z = 274.52	8438.476	108.942	1996.009	2150.604!	524.729	135.800		Not harmful

Notes: Green: Not harmful; Yellow: Harmful; Orange: Toxic; Red: Very toxic

According to toxicity assessment levels of the Globally Harmonized System of Classification and Labeling of Chemicals, the four levels include:

Not harmful ($LC_{50}/EC_{50}/ChV > 100$ mg/L),

Harmful (10 mg/L $< LC_{50}/EC_{50}/ChV \leq 100$ mg/L),

Toxic (1 mg/L $< LC_{50}/EC_{50}/ChV \leq 10$ mg/L),

Very toxic ($LC_{50}/EC_{50}/ChV \leq 1$ mg/L).

The lowest acute toxicity values between and with different species are used to define the appropriate hazard category of the compounds.

*** = asterisk designates: Chemical may not be soluble enough to measure this predicted effect. If the effect level exceeds the water solubility by 10X, typically no effects at saturation (NES) are reported.**

! = exclamation designates: The toxicity value was estimated through application of acute-to-chronic ratios per methods outlined in the ECOSAR Methodology Document provided in the ECOSAR Help Menu.

References

1 G. Kresse and J. Furthmüller, Efficient iterative schemes for Ab Initio total-energy calculations using a plane-wave basis set, *Phys. Rev. B*, 1996, 54, 11169–11186.

2 J. P. Perdew, K. Burke and M. Ernzerhof, Generalized gradient

approximation made simple, *Phys. Rev. Lett.*, 1996, 77, 3865–3868.

3 S. Grimme, J. Antony, S. Ehrlich and H. Krieg, A consistent and accurate Ab initio parametrization of density functional dispersion correction (DFT-D) for the 94 elements H-Pu, *J. Chem. Phys.*, 2010, 132, 154104.

4 Y. Qin, J. Luo, Q. An, Z. Xiao, J. Hao, Y. Tong and S. Zhai, Three-dimensional Co–N/SBA-15/alginate hydrogels with excellent recovery and recyclability for activating peroxymonosulfate to degrade ciprofloxacin, *Microporous Mesoporous Mater.*, 2021, 323, 111259.

5 Y. Huang, L. Nengzi, X. Zhang, J. Gou, Y. Gao, G. Zhu, Q. Cheng and X. Cheng, Catalytic degradation of ciprofloxacin by magnetic CuS/Fe_2O_3/Mn_2O_3 nanocomposite activated peroxymonosulfate: influence factors, degradation pathways and reaction mechanism, *Chem. Eng. J.*, 2020, 388, 124274.

6 H. Luo, C. Ni, C. Zhang, W. Wang, Y. Yang, W. Xiong, M. Cheng, C. Zhou, Y. Zhou, S. Tian, Q. Lin, G. Fang, Z. Zeng and G. Zeng, Lignocellulosic biomass derived N-doped and CoO-loaded carbocatalyst used as highly efficient peroxymonosulfate activator for ciprofloxacin degradation, *J. Colloid Interface Sci.*, 2022, 610, 221–233.

7 F. Chen, G.-X. Huang, F.-B. Yao, Q. Yang, Y.-M. Zheng, Q.-B. Zhao and H.-Q. Yu, Catalytic degradation of ciprofloxacin by a visible-light-assisted peroxymonosulfate activation system: performance and mechanism, *Water Res.*, 2020, 173, 115559.

8 Y. You, Z. Zhao, Y. Song, J. Li, J. Li and X. Cheng, Synthesis of magnetized nitrogen-doped biochar and its high efficiency for elimination of ciprofloxacin hydrochloride by activation of peroxymonosulfate, *Sep. Purif. Technol.*, 2021, 258, 117977.

9 C.-H. Shen, X.-J. Wen, Z.-H. Fei, Z.-T. Liu and Q.-M. Mu, Visible-light-driven activation of peroxymonosulfate for accelerating ciprofloxacin degradation using CeO_2/Co_3O_4 p-n heterojunction photocatalysts, *Chem. Eng. J.*, 2020, 391, 123612.

10 M.-M. Chen, H.-Y. Niu, C.-G. Niu, H. Guo, S. Liang and Y.-Y. Yang, Metal-

organic framework-derived CuCo/carbon as an efficient magnetic heterogeneous catalyst for persulfate activation and ciprofloxacin degradation, *J. Hazard. Mater.*, 2022, 424, 127196.

11 B. He, L. Song, Z. Zhao, W. Liu, Y. Zhou, J. Shang and X. Cheng, $CuFe_2O_4$/CuO magnetic nano-composite activates pms to remove ciprofloxacin: ecotoxicity and DFT calculation, *Chem. Eng. J.*, 2022, 446, 137183.

12 H. D. Chen, J. K. Xu, J. Q. Wei, P. F. Wang, Y. B. Han, J. C. Xu, B. Hong, H. X. Jin, D. F. Jin, X. L. Peng, J. Li, Y. T. Yang, H. L. Ge and X. Q. Wang, Mesoporous $CoFe_2O_4$ nanowires: nanocasting synthesis, magnetic separation and enhanced catalytic degradation for ciprofloxacin, *J. Phys. Chem. Solids*, 2019, 132, 138–144.